Studies of differential and total photoionization cross sections of molecular nitrogen

Robert R. Lucchese, Georges Raseev,* and Vincent McKoy
Arthur Amos Noyes Laboratory of Chemical Physics, California Institute of Technology, Pasadena, California 91125
(Received 9 July 1981)

The photoionization of molecular nitrogen has been studied using a frozen-core Hartree-Fock final-state wave function with a correlated intitial-state wave function. The final-state wave function was obtained using the iterative Schwinger variational method. The effects of initial-state correlation were studied by comparing cross sections obtained using a configuration-interaction-type initial-state wave function with those obtained using a Hartree-Fock initial-state wave function. In this paper we compare our accurate single-center expansion results with other theoretical results. We find that earlier single-center cross sections were not well converged with respect to their expansion parameters. The results of the continuum multiple-scattering method and the Stieltjes-Tchebycheff moment-theory approach are found to be in qualitative but not quantitative agreement with the present results. We also compare our computed total cross sections as well as integrated target angular distributions with experimental results for photoionization leading to the $X\,^2\Sigma_g^+$, $A\,^2\Pi_u$, and $B\,^2\Sigma_u^+$ states of N_2^+. We find generally good agreement, which is improved by the inclusion of initial-state correlation effects, especially in the resonant photoionization channel leading to the $X\,^2\Sigma_g^+$ state of N_2^+. We also report integrated detector angular distributions for these three channels.

I. INTRODUCTION

The photoionization of molecular systems is a topic of much current theoretical interest.[1] As a prototypical system, the photoionization of molecular nitrogen has been studied using several different methods including the continuum multiple-scattering method (CMSM),[2] the Stieltjes-Tchebycheff moment-theory approach (STMT), both in the Hartree-Fock (HF) approximation[3,4] and the random-phase approximation with exchange (RPAE),[5] and several numerical single-center expansion methods.[6] The single-center expansion methods applied to the photoionization of molecular nitrogen have treated the interaction potential in several different ways. There have been static and static-plus-orthogonalization calculations,[7] static-plus-model-exchange calculations,[8] and exact static-exchange calculations.[9,10] Most previous studies have attempted to obtain the continuum solution for the final state using the frozen-core Hartree-Fock (FCHF) approximation.[9] The present study is directed at obtaining accurate and converged FCHF solutions for the final-state wave function, using the body-fixed frame, fixed nuclei approach.[6] We compare our results with some of the other theoretical results mentioned above and with the experimental results of continuous source experiments by Plummer *et al.*[11] and Marr *et al.*[12] using synchrotron radiation, and by Hamnett *et al.*[13] and Wight *et al.*[14] obtained using an $(e,2e)$ technique.

We have considered the photoionization leading to the $X\,^2\Sigma_g^+$, $A\,^2\Pi_u$, and $B\,^2\Sigma_u^+$ states of N_2^+. Both total and partial photoionization cross sections and angular distributions for these states are reported. Following the suggestion of Wallace and Dill,[15] we give both the asymmetry parameter for the usual integrated target angular distribution (ITAD), denoted here by $\beta_{\hat{k}}$, and the integrated detector angular distribution (IDAD), denoted by $\beta_{\hat{n}}$. In combination with accurate FCHF final-state wave functions, we have considered the effect of initial-state correlation by comparing the results obtained using both HF and configuration-interaction-type (CI) initial-state wave functions. The difference between the dipole length and dipole velocity forms of the cross sections is used to estimate the remaining final-state correlation effects.

We solve the static-exchange continuum equations using the iterative Schwinger method.[16,17] This method is essentially a single-center expansion

technique comparable to the methods used by Raseev *et al.*[9] and Robb and Collins.[10] The iterative Schwinger method has been earlier applied to the photoionization of H_2 and CO_2 (Refs. 18 and 19) as well as to electron-molecule collisions for the e-H_2, e-LiH, and e-CO_2 systems.[16,20,21] We find in this study of the photoionization of N_2 that the iterative Schwinger method converges rapidly.

The present results are compared with the results of other single-center expansion methods. We find that, for the shape resonance in the photoionization channel leading to the $X\,^2\Sigma_g^+$ state of N_2^+, the previous results of Raseev *et al.*[9] and Robb *et al.*[10] are not well converged. In particular, their peak cross section occurs at a photon energy of 31 eV which differs from the present result of 29 eV. In this regard, we have determined empirically that the energy of the peak cross section in this shape resonance, for which the continuum function is of σ_u symmetry, converges as

$$E^l_{\max}-E^{\infty}_{\max}\propto\frac{1}{l^3}\ , \tag{1}$$

where l is the maximum l included in the partial-wave expansion of the continuum function. We also compare our accurate static-exchange results with the results obtained using the CMSM and STMT methods.[2–4] This comparison shows that the CMSM and STMT results are qualitatively similar to accurate static-exchange results but neither the CMSM nor STMT is in quantitative (better than 10%) agreement with the present results. Finally, the comparison with experimental results[11–14] shows that the FCHF final-state model reproduces the experimental cross section well except in the energy regions where two-electron resonances, such as autoionization, are important.

We find that the inclusion of initial-state correlation brings the dipole length and velocity forms of the photoionization cross section into better agreement with experimental results. This result for molecular systems is similar to that found by Swanson and Armstrong for atomic systems.[22] In the region of the shape resonance leading to the $X\,^2\Sigma_g^+$ state of N_2^+, the combination of the correlated intitial-state wave function and the FCHF final-state wave function is found to be particularly effective.

II. METHOD

A. Iterative Schwinger variational method

We compute the final-state photoionization wave functions using the FCHF approximation.[9] This implies that the final state is described by a single electronic configuration in which the ionic core orbitals are constrained to be identical to the HF orbitals of the neutral molecule. The Schrödinger equation for the remaining continuum orbital is then (in atomic units)

$$\left[-\tfrac{1}{2}\nabla^2-\frac{1}{r}+V(\vec{r})-\frac{k^2}{2}\right]\Psi^{(\pm)}_{\vec{k}}(\vec{r})=0\ , \tag{2}$$

where $V(\vec{r})$ is the short-range portion of the static-exchange potential, and $\vec{k}$ is the momentum of the continuum electron. By using the FCHF approximation, the final-state photoionization problem is reduced to solving a single-particle potential scattering problem.

The Schrödinger equation given in Eq. (2) is equivalent to the Lippmann-Schwinger equation

$$\Psi^{(\pm)}_{\vec{k}}=\Psi^{c(\pm)}_{\vec{k}}+G^{c(\pm)}U\Psi^{(\pm)}_{\vec{k}}\ , \tag{3}$$

where $U(\vec{r})=2V(\vec{r})$, and $G^{c(\pm)}$ is the Coulomb Green's function defined by

$$G^{c(\pm)}=\left[\nabla^2+\frac{2}{r}+k^2\pm i\epsilon\right]^{-1}\ . \tag{4}$$

The function $\Psi^{c(\pm)}_{\vec{k}}$ is the pure Coulomb scattering function and is given in terms of its partial-wave expansion as

$$\Psi^{c(\pm)}_{\vec{k}}(\vec{r})=\left[\frac{2}{\pi}\right]^{1/2}\sum_{l,m} i^l\phi^{c(\pm)}_{klm}(\vec{r})Y^*_{lm}(\Omega_{\hat{k}})\ , \tag{5}$$

where $\phi^{c(\pm)}$ is the partial-wave Coulomb function defined by

$$\phi^{c(\pm)}_{klm}(\vec{r})=e^{\pm i\sigma_l}\frac{F_l(\gamma;kr)}{kr}Y_{lm}(\Omega_{\hat{r}})\ . \tag{6}$$

The function $F_l(\gamma;kr)$ is the regular Coulomb function, with $\gamma=-1/k$, and σ_l is the Coulomb phase shift defined as $\sigma_l=\arg[\Gamma(l+1+i\gamma)]$.[23]

The wave function $\Psi^{(-)}_{\vec{k}}$, which represents the ejected electron with momentum $\vec{k}$, is then expanded in the partial-wave series

$$\Psi^{(-)}_{\vec{k}}(\vec{r})=\left[\frac{2}{\pi}\right]^{1/2}\sum_{l=0}^{l_p}\sum_{m=-l}^{+l} i^l\psi^{(-)}_{klm}(\vec{r})Y^*_{lm}(\Omega_{\hat{k}})\ , \tag{7}$$

where an infinite sum over l's has been truncated at $l=l_p$. Computing the wave function in the partial-wave form allows the dependence of the scattering solution on the target orientation to be

treated analytically. The Lippmann-Schwinger equation for the partial-wave states is then

$$\psi_{klm}^{(-)}(\vec{r})=\phi_{klm}^{c(-)}(\vec{r})+\langle \vec{r} \mid G^{c(-)}U \mid \psi_{klm}^{(-)}\rangle \ . \quad (8)$$

We solve Eq. (8) using an iterative procedure.[16] The iterative method begins by approximating the short-range potential by a separable potential of the form

$$\langle \vec{r} \mid U^{S_0} \mid \vec{r}' \rangle = \sum_{\alpha_i,\alpha_j \in R} \langle \vec{r} \mid U \mid \alpha_i \rangle [pU^{-1}]_{ij} \langle \alpha_j \mid U \mid \vec{r}' \rangle \ , \quad (9)$$

where R is some initial set of expansion functions and $[U^{-1}]_{ij}$ is the matrix inverse of U_{ij}. Inserting this approximation to U in to Eq. (8) allows the Lippmann-Schwinger equation to be solved since the kernel of the integral equation is now separable.[24] The solution to Eq. (8) with the potential approximated by U^{S_0} is

$$\psi_{klm}^{(-)S_0}(\vec{r})= \phi_{klm}^{c(-)}(\vec{r}) + \sum_{\alpha_i,\alpha_j \in R} \langle \vec{r} \mid G^{c(-)}U \mid \alpha_i \rangle [D^{-1}]_{ij} \times \langle \alpha_j \mid U \mid \phi_{klm}^{c(-)} \rangle \ , \quad (10)$$

where

$$D_{ij}=\langle \alpha_i \mid U-UG^{c(-)}U \mid \alpha_j \rangle \ . \quad (11)$$

The use of a separable potential of the form given in Eq. (9) to solve the Lippmann-Schwinger equation is known to be identical to the use of the Schwinger variational expression,[25–27] and hence we call this method the iterative Schwinger variational method.

The iterative method is continued by augmenting the expansion set R, of Eq. (9), by the set of functions

$$S_0=\{\psi_{kl_1m}^{S_0}, \psi_{kl_2m}^{S_0},\ldots,\psi_{kl_pm}^{S_0}\} \ , \quad (12)$$

which are the scattering solutions given by Eq. (10), and where l_p is the maximum l included in the expansion of the scattering solution as given in Eq. (7). Using this augmented set of functions, a second set of scattering solutions

$$S_1=\{\psi_{kl_1m}^{S_1},\ldots,\psi_{kl_pm}^{S_1}\}$$

is obtained using Eq. (10). In general, the set of scattering solutions at the nth iteration

$$S_n=\{\psi_{kl_1m}^{S_n},\ldots,\psi_{kl_pm}^{S_n}\} \quad (13)$$

is obtained from the previous set of solutions S_{n-1} from

$$\psi_{klm}^{(-)S_n}(\vec{r})=\phi_{klm}^{c(-)}(\vec{r}) + \sum_{\chi_i,\chi_j \in R \cup S_{n-1}} \times \langle \vec{r} \mid G^{c(-)}U \mid \chi_i \rangle [D^{-1}]_{ij} \times \langle \chi_j \mid U \mid \phi_{klm}^{c(-)} \rangle \ . \quad (14)$$

This iterative procedure is continued until the wave functions converge. When the wave functions do converge, it can be shown that they are solutions of the Lippmann-Schwinger equation for the exact potential U.[16]

B. Frozen-core Hartree-Fock static-exchange potential

In this section we will discuss the form of the static-exchange potential, obtained from the FCHF approximation, which describes the interaction of the ionized electron with the open-shell ionic core.[28] First consider the HF wave function of a closed-shell molecule such as N_2. The HF wave function is simply written as a single Slater determinant

$$\Psi= \mid \phi_1\alpha\phi_1\beta\cdots\phi_n\alpha\phi_n\beta \mid \ . \quad (15)$$

The photoionization final-state wave function in the FCHF approximation, where the ionized electron is removed from orbital ϕ_n, is written as

$$\Psi_{\vec{k}}=(\tfrac{1}{2})^{1/2}\{ \mid \phi_1\alpha\phi_1\beta\cdots\phi_n\alpha\phi_{\vec{k}}\beta \mid + \mid \phi_1\alpha\phi_1\beta\cdots\phi_{\vec{k}}\alpha\phi_n\beta \mid \} \ , \quad (16)$$

assuming that ϕ_n is a nondegenerate orbital. Then the correct single-particle equation for the continuum electron is obtained from

$$\langle \delta\Psi_{\vec{k}} \mid H-E \mid \Psi_{\vec{k}} \rangle =0 \ , \quad (17)$$

where

$$\delta\Psi_{\vec{k}}=(\tfrac{1}{2})^{1/2}\{ \mid \phi_1\alpha\phi_1\beta\cdots\phi_n\alpha\delta\phi_{\vec{k}}\beta \mid + \mid \phi_1\alpha\phi_1\beta\cdots\delta\phi_{\vec{k}}\alpha\phi_n\beta \mid \} \ , \quad (18)$$

and where Eq. (17) holds for all possible $\delta\phi_{\vec{k}}$.

The electronic Hamiltonian can be written as

$$H=\sum_{i=1}^{N} f(i)+\sum_{i<j}^{N}\frac{1}{r_{ij}}\ , \tag{19}$$

with

$$f(i)=-\tfrac{1}{2}\nabla_i^2-\sum_{\alpha}\frac{Z_\alpha}{r_{i\alpha}}\ , \tag{20}$$

where Z_α are the nuclear charges, and $N=2n$ is the number of electrons. The one-electron HF Hamiltonian can be written in this form as

$$H^{\mathrm{HF}}=f+\sum_{i=1}^{n} 2J_i-K_i\ , \tag{21}$$

where f is the one-electron operator defined in Eq. (20), and J_i and K_i are the usual Coulomb and exchange operators.[29] Thus the HF orbitals satisfy

$$H^{\mathrm{HF}}\phi_n=\epsilon_n\phi_n\ . \tag{22}$$

If we assume that the orbitals $\phi_{\vec{k}}$ and $\delta\phi_{\vec{k}}$ are not necessarily orthogonal to each other nor to the orthonormal set of occupied HF orbitals, then Eq. (17) can be expanded to give

$$\begin{aligned}0=&\langle(P\delta\phi_{\vec{k}})\,|\,\tilde{H}-\epsilon+J_n+K_n\,|\,P\phi_{\vec{k}}\rangle+2\langle\delta\phi_{\vec{k}}\,|\,\phi_n\rangle\langle\phi_n\,|\,\tilde{H}-\epsilon+J_n\,|\,\phi_n\rangle\langle\phi_n\,|\,\phi_{\vec{k}}\rangle\\&+2\langle\delta\phi_{\vec{k}}\,|\,\phi_n\rangle\langle\phi_n\,|\,\tilde{H}+J_n\,|\,P\phi_{\vec{k}}\rangle+2\langle(P\delta\phi_{\vec{k}})\,|\,\tilde{H}+J_n\,|\,\phi_n\rangle\langle\phi_n\,|\,\phi_{\vec{k}}\rangle\ ,\end{aligned} \tag{23}$$

where

$$\tilde{H}=f+\sum_{i=1}^{n-1} 2J_i-K_i \tag{24}$$

and

$$P=1-\sum_{i=1}^{n}|\,\phi_i\rangle\langle\phi_i\,|\ . \tag{25}$$

The energy of the continuum electron is

$$\epsilon=E-E^{\mathrm{core}}\ , \tag{26}$$

where E^{core} is the Koopman's theorem energy of the ionic core

$$E^{\mathrm{core}}=E^{\mathrm{HF}}-\epsilon_n\ . \tag{27}$$

The fact that ϕ_n is an eigenfunction of H^{HF} [Eq. (22)], reduces Eq. (23) to[30]

$$\begin{aligned}0=&\langle(P\delta\phi_{\vec{k}})\,|\,\tilde{H}-\epsilon+J_n+K_n\,|\,P\phi_{\vec{k}}\rangle\\&+2(\epsilon_n-\epsilon)\langle\delta\phi_{\vec{k}}\,|\,\phi_n\rangle\langle\phi_n\,|\,\phi_{\vec{k}}\rangle\ ,\end{aligned} \tag{28}$$

which must hold for all $\delta\phi_{\vec{k}}$. If we consider the case where $\delta\phi_{\vec{k}}=\phi_n$, then it follows that if $\epsilon\neq\epsilon_n$ then $\langle\phi_{\vec{k}}\,|\,\phi_n\rangle=0$. Thus, if $\phi'_{\vec{k}}$ satisfies

$$0=\langle(P\delta\phi'_{\vec{k}})\,|\,\tilde{H}-\epsilon+J_n+K_n\,|\,P\phi'_{\vec{k}}\rangle \tag{29}$$

for all $\delta\phi'_{\vec{k}}$ and with $\epsilon\neq\epsilon_n$, then $\phi_{\vec{k}}=P\phi'_{\vec{k}}$ satisfies Eq. (28). So, solving Eq. (29) will give us the correct continuum wave function in the FCHF approximation.

There are several points to note about Eq. (29). First, Eq. (29) constrains the solution $P\phi'_{\vec{k}}$ to be orthogonal to the occupied orbitals. Thus, this form of the scattering equation is entirely equivalent to the standard undetermined Lagrange multiplier form[10,31]

$$(\tilde{H}-\epsilon+J_n+K_n)\phi_{\vec{k}}=\sum_{i=1}^{n}\lambda_i\phi_i\ , \tag{30}$$

where λ_i are undetermined multipliers, and $\phi_{\vec{k}}$ is subject to the condition

$$\langle\phi_{\vec{k}}\,|\,\phi_i\rangle=0,\quad i=1,2,\ldots,n\ . \tag{31}$$

Secondly, the continuum solution *must* be constrained to be orthogonal to the doubly occupied orbitals since, unlike in the electron-neutral closed-shell HF scattering case, the continuum orbital and the occupied orbitals are not eigenfunctions of the same one-electron Hamiltonian. Lastly, the general open-shell scattering problem would require the solution of Eq. (23), but as we have seen, since we are using the FCHF approximation, the scattering equations can be simplified to yield Eq. (29).

A scattering equation of the form of Eq. (2) can be obtained from Eq. (29) giving

$$(-\tfrac{1}{2}\nabla^2+V^{\mathrm{orth}}-\epsilon)\phi_{\vec{k}}=0\ . \tag{32}$$

The potential V^{orth} is a generalized Phillips-Kleinman pseudopotential[32]:

$$V^{\mathrm{orth}}=V-LQ-QL+QLQ\ , \tag{33}$$

where L, Q, and V are defined by

$$L=-\tfrac{1}{2}\nabla^2-\epsilon+V\ , \tag{34}$$

$$Q=\sum_{i=1}^{n}|\,\phi_i\rangle\langle\phi_i\,|\ , \tag{35}$$

and

$$V=\sum_{i=1}^{n-1}(2J_i-K_i)+J_n+K_n-\sum_{\alpha}\frac{Z_\alpha}{r_{i\alpha}} . \quad (36)$$

Thus, we us the pseudopotential V^{orth} to treat both the static-exchange interaction and the effects of constraining the continuum solution to be orthogonal to the occupied bound orbitals.

C. Photoionization cross sections and asymmetry parameters

The photoionization cross section for going from an initial bound state Ψ_i to the continuum state $\Psi_{f,\vec{k}}$ due to linearly polarized light in the dipole length and dipole velocity approximations is proportional to the square of the dipole matrix elements

$$I^L_{\vec{k},\hat{n}}=(k)^{1/2}\langle\Psi_i\,|\,\vec{r}\cdot\hat{n}\,|\,\Psi^{(-)}_{f,\vec{k}}\rangle \quad (37)$$

for the dipole length form, and

$$I^V_{\vec{k},\hat{n}}=\frac{(k)^{1/2}}{E}\langle\Psi_i\,|\,\vec{\nabla}\cdot\hat{n}\,|\,\Psi^{(-)}_{f,\vec{k}}\rangle \quad (38)$$

for the velocity form. In Eqs. (37) and (38), E is the photon energy, $\hat{n}$ is the direction of polarization of the light, and $\vec{k}$ is the momentum of the photoelectron. The factor of $(k)^{1/2}$ in Eqs. (37) and (38) is required to change the normalization of the continuum functions, $\Psi^{(-)}_{f,\vec{k}}$, from momentum to energy normalized. The doubly differential photoionization cross sections in the body-fixed frame is then

$$\frac{d^2\sigma^{L,V}}{d\Omega_{\hat{k}}d\Omega_{\hat{n}}}=\frac{4\pi^2E}{c}\,|\,I^{L,V}_{\vec{k},\hat{n}}\,|^2 . \quad (39)$$

If the wave functions used to calculate the photoionization cross section were exact eigenfunctions of the electronic Hamiltonian, then the dipole length and dipole velocity forms of the cross section would be equivalent. Thus, the equality of these two forms is a necessary but not sufficient condition that the computed cross sections are accurate. In this sense, the difference between the length and velocity forms can be viewed as an estimate of the minimum error in the calculation.[22,33]

To treat the angular dependence of the cross section on the target orientation, the dipole matrix elements are expanded in terms of spherical harmonics

$$I^{L,V}_{\vec{k},\hat{n}}=\left[\frac{4\pi}{3}\right]^{1/2}\sum_{lm\mu}I^{L,V}_{lm\mu}Y^*_{lm}(\Omega_{\hat{k}})Y^*_{1\mu}(\Omega_{\hat{n}}) . \quad (40)$$

The partial-wave matrix elements are then given by

$$I^L_{lm\mu}=(k)^{1/2}\langle\Psi_i\,|\,r_\mu\,|\,\Psi^{(-)}_{f,klm}\rangle \quad (41)$$

for the dipole length form, and

$$I^V_{lm\mu}=\frac{(k)^{1/2}}{E}\langle\Psi_i\,|\,\nabla_\mu\,|\,\Psi^{(-)}_{f,klm}\rangle \quad (42)$$

for the dipole velocity form, where

$$r_\mu=\begin{cases}\mp(x\pm iy)/2^{1/2} & \text{for } \mu=\pm1 ,\\ z & \text{for } \mu=0 ,\end{cases} \quad (43)$$

and

$$\nabla_\mu=\begin{cases}\mp\left(\dfrac{\partial}{\partial x}\right)\pm i\left[\dfrac{\partial}{\partial y}\right]/2^{1/2} & \text{for } \mu=\pm1 ,\\ \dfrac{\partial}{\partial z} & \text{for } \mu=0 .\end{cases} \quad (44)$$

The total photoionization cross section averaged over all polarizations and photoelectron directions is then

$$\sigma^{L,V}=\frac{4\pi^2}{3c}E\left[\sum_\mu D_\mu\right] , \quad (45)$$

where

$$D_\mu=\sum_l\,|\,I^{L,V}_{l,\Delta m-\mu,\mu}\,|^2 . \quad (46)$$

Note that for linear molecules we have

$$\Delta m=m(\Psi_i)-m(\mathscr{i})=\mu+m(\mathscr{k}) , \quad (47)$$

where $\mathscr{i}$ represents ion core and $\mathscr{k}$ represents the photoelectron. There are two other averaged photoionization cross sections of interest as suggested by Wallace and Dill.[15] The first is the usual integrated target angular distribution (ITAD). The ITAD corresponds to the photoionization experiment where the target orientation is not resolved. This is the form of the photoionization cross section measured in the usual gas phase experiment. When the cross section in Eq. (39) is averaged over all target orientations the ITAD is found to be of the form

$$\frac{d\sigma^{L,V}}{d\Omega_{\hat{k}}}=\frac{\sigma^{L,V}}{4\pi}[1+\beta^{L,V}_{\hat{k}}P_2(\cos\theta)] . \quad (48)$$

The angle θ is the angle between the direction of polarization of the light and the momentum of the electron, and $P_2(\cos\theta)$ is the Legendre polynomial of degree 2. The asymmetry parameter $\beta_{\hat{k}}$ is given by[34]

$$\beta_{\hat{k}}^{L,V}=\frac{3}{5}\left[1/\sum_{\mu}D_{\mu}\right]\sum_{\substack{lm\mu\\ l'm'\mu'\\ \mu''}}(-1)^{m-\mu'}I_{lm\mu}^{L,V}(I_{l'm'\mu'}^{L,V})^{*}[(2l+1)(2l'+1)]^{1/2}(1100\,|\,20)$$
$$\times(ll'00\,|\,20)(11-\mu\mu'\,|\,2\mu'')(ll'-m-m'\,|\,2-\mu'')\ , \tag{49}$$

where $(j_1j_2m_1m_2\,|\,j_3m_3)$ is a Clebsch-Gordan coefficient. Note that the asymmetry parameter $\beta_{\hat{k}}$ depends only on the photon energy and that the subscript $\hat{k}$ implies only that $\beta_{\hat{k}}$ describes the distribution of the photoelectrons and not that $\beta_{\hat{k}}$ depends on their direction. The second averaged photoionization cross section we will consider is the integrated detector angular distribution (IDAD). The IDAD corresponds to the experiment where the target orientation is fixed in the laboratory frame of reference and the cross section is then integrated over all possible directions of emission of the photoelectron. Wallace and Dill[15] have suggested that the IDAD cross section would be useful in determining the orientation of a photoionized target in the laboratory frame. When the cross section given in Eq. (39) is integrated over all photoelectron directions, the IDAD is found to be of the form

$$\frac{d\sigma^{L,V}}{d\Omega_{\hat{n}}}=\frac{\sigma^{L,V}}{4\pi}[1+\beta_{\hat{n}}^{L,V}P_2(\cos\theta)]\ . \tag{50}$$

The angle θ in this case is the angle between the direction of the polarization of the light and the molecular z axis. The asymmetry parameter $\beta_{\hat{n}}$ is given by

$$\beta_{\hat{n}}^{L,V}=[2D_0-(D_{-1}+D_{+1})]/\left[\sum_{\mu}D_{\mu}\right]\ . \tag{51}$$

III. RESULTS AND DISCUSSION

A. Final-state wave functions

The final-state wave functions used in this study of photoionization are constructed using the FCHF approximation. The bound orbitals in this approximation come from the HF wave function of the neutral molecule. We have constructed a HF wave function for the neutral N_2 molecule using a double-zeta plus d functions contracted Gaussian basis of the form $(9s\,5p\,2d/4s\,3p\,2d)$.[35,36] The d-function exponents are 1.5836 and 0.4691 which are the exponents appropriate to representing a Slater function with exponent $\xi=2.20$.[36] The bond length was taken as 2.068 a.u. The HF energy for this basis set is $E=-108.973\,235$ a.u., and the quadrupole moment for the neutral N_2 molecule in the basis set is $\theta_{zz}=-0.9923$ a.u. (Ref. 36).

To compute the final-state continuum wave function we must evaluate the various matrix elements given in Eq. (14). We have used a single-center expansion approach to evaluate all such matrix elements.[6,30,37] The use of single-center techniques implies that all functions (e.g., scattering functions, occupied orbitals, $1/r_{12}$, $G^{c(-)}$) are expanded about a common origin (taken to be the bond center for N_2) as a sum of spherical harmonics times radial functions. The radial integrals are computed by putting the radial functions on a grid and then using Simpson's rule. The angular integrals can then be done analytically. Actual calculations use standing-wave boundary conditions thus allowing radial wave functions to be represented by real-valued functions.

There are several parameters which describe the maximum l included in such spherical harmonic expansions. Using a notation similar to that of Robb and Collins,[10,38] we define our expansion parameters as follows:

(1) $l_m=$ maximum l included in the expansion of scattering functions [χ_i's of Eq. (14)], of the Coulomb Green's function, and of the projection orbitals [ϕ_i of Eq. (35)].

(2) $l_s^{\rm ex}=$ maximum l included in the expansion of the scattering functions in the exchange terms.

(3) $l_i^{\rm ex}=$ maximum l included in the expansion of the occupied orbitals in the exchange terms.

(4) $l_i^{\rm dir}=$ maximum l included in the expansion of the occupied orbitals in the direct potential.

(5) $\lambda_m^{\rm em}=$ maximum l included in the expansion of $1/r_{12}$ in the exchange terms.

(6) $\lambda_m^{\rm dir}=$ maximum l included in the expansion of $1/r_{12}$ in the direct potential (not including the nuclear terms).

Also note that we always include terms up to $\lambda=2l_m$ in the expansion of the nuclear potential. We have expanded all radial integrands on a grid of 800 points extending to $r=64.0$ a.u. The smallest step size in this grid is 0.01 a.u. which is used

out to $r=2.0$ a.u. The largest step size is 0.16 a.u.

For the purposes of this study we have grouped the six parameters listed above as follows:

(i) $l_{\max}^{\text{dir}}=l_m,l_i^{\text{dir}},\lambda_m^{\text{dir}}$;

(ii) $l_{\max}^{\text{exc}}=l_s^{\text{ex}},\lambda_m^{\text{ex}}$.

For all calculations on N_2 considered here we have fixed l_i^{ex} to be $l_i^{\text{ex}}=16(1\sigma_g)$, $10(2\sigma_g)$, $10(3\sigma_g)$, $15(1\sigma_u)$, $9(2\sigma_u)$, $9(1\pi_u)$. These values correspond to having normalized the expansions of the various orbitals to better than 0.99.

To study the general convergence in this system we have intitially considered four sets of parameters:

(A) $l_{\max}^{\text{dir}}=20$, $l_{\max}^{\text{exc}}=20$,

(B) $l_{\max}^{\text{dir}}=30$, $l_{\max}^{\text{exc}}=20$,

(C) $l_{\max}^{\text{dir}}=40$, $l_{\max}^{\text{exc}}=20$,

(D) $l_{\max}^{\text{dir}}=30$, $l_{\max}^{\text{exc}}=30$.

We have used these four sets of parameters to calculate the photoionization cross section in the $3\sigma_g\rightarrow k\sigma_u$ channel of N_2. This channel was chosen since it contains a shape resonance which makes the computed cross section more sensitive to the parameters of the potential than in a nonresonant channel. The results for parameter sets A, B, and C are shown in Fig. 1. On the scale shown in Fig. 1, the cross section with parameter set D cannot be distinguished from that of set B. The difference between sets B and C is less than 5% in the cross section. We consider the accuracy of set B to be adequate considering the FCHF approximation within which we are computing these cross sections. Thus, except where noted, we have used this set of parameters with $l_{\max}^{\text{dir}}=30$ and $l_{\max}^{\text{exc}}=20$ for all other calculations in this study. A more detailed discussion of the convergence of the energy peak cross sections in the $3\sigma_g\rightarrow k\sigma_u$ channel is given in Sec. III C of this paper.

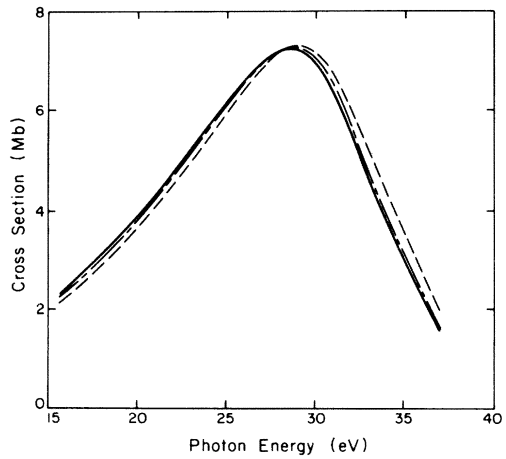

FIG. 1. Convergence of the $3\sigma_g\rightarrow k\sigma_u$ photoionization cross section of N_2 with varying potential parameters: — — — parameter set A ($l_{\max}^{\text{dir}}=20$); —·—· parameter set B ($l_{\max}^{\text{dir}}=30$); —— parameter set C ($l_{\max}^{\text{dir}}=40$). For all three sets $l_{\max}^{\text{exc}}=20$. These are results of noniterative calculations using the σ_u basis set of Table I in Eq. (10). One megabarn (Mb) is 10^{-18} cm^2.

The scattering basis sets, corresponding to the set R of Eq. (10), which were used to obtain scattering solutions of the various possible symmetries, are given in Table I. The basis sets are constructed both from Cartesian Gaussian functions which are of the form

$$\phi(\vec{r})^{\alpha,l,m,n,\vec{A}} =N(x-A_x)^l(y-A_y)^m(z-A_z)^n e^{-\alpha|\vec{r}-\vec{A}|^2} \tag{52}$$

centered at the nuclei, and spherical Gaussians of the form

$$\phi(\vec{r})^{\alpha,l,m,\vec{A}} =N|\vec{r}-\vec{A}|^l e^{-\alpha|\vec{r}-\vec{A}|^2}Y_{lm}(\Omega_{\vec{r}-\vec{A}}) \tag{53}$$

centered at the expansion origin. We have examined the rate of convergence of the iterative Schwinger variational method with basis sets of this size. In Fig. 2 we present the results of photoionization calculations in the $3\sigma_g\rightarrow k\sigma_u$ channel using the σ_u basis set given in Table I. The cross section without iteration [Eq. (10)] and from the first iteration [Eq. (14) with $n=1$] are both given in Fig. 2. The cross section obtained from the second iteration is indistinguishable from that given for the first iteration on the scale presented in Fig. 2. Thus, for all other channels we have only presented cross sections from the results of the first iteration. We have assured the adequacy of the basis sets for the other scattering symmetries, given in Table I, by comparing the zero-iteration cross section to the one-iteration cross section. In all the other channels considered here, this difference is small and of the same order as that we have obtained in the $3\sigma_g\rightarrow k\sigma_u$ channel.

B. Initial-state wave function

Swanson and Armstrong[22] found that inclusion of correlation effects in the initial-state wave func-

TABLE I. Scattering basis sets used with the Schwinger variational expression.[a]

Symmetry of continuum solution	Type of Gaussian function[b]		Exponents
σ_g	Cartesian	s	16.0,8.0,4.0,2.0,1.0,0.5
		z	1.0,0.5
	Spherical	$l=0$	2.0,1.0,0.5
		$l=2$	2.0,1.0,0.5
σ_u	Cartesian	s	16.0,8.0,4.0,2.0,1.0,0.5
		z	1.0,0.5
	Spherical	$l=1$	4.0,2.0,1.0,0.5
		$l=3$	4.0,2.0,1.0,0.5
		$l=5$	1.0,0.5
π_u	Cartesian	x	8.0,4.0,2.0,1.0,0.5
		xz	0.5
	Spherical	$l=1$	1.0
		$l=3$	1.0
π_g	Cartesian	x	8.0,4.0,2.0,1.0,0.5
		xz	0.5
	Spherical	$l=2$	1.0
		$l=4$	1.0
δ_g	Cartesian	xy	4.0,2.0,1.0,0.5,0.25
	Spherical	$l=2$	1.0
		$l=4$	1.0

[a]These basis sets correspond to the set R of Eq. (10).
[b]The basis functions are symmetry adapted functions constructed from either Cartesian or spherical Gaussian functions, as defined in the text, of the given type. Cartesian functions are centered at the nuclei and spherical functions are centered at the bond midpoint.

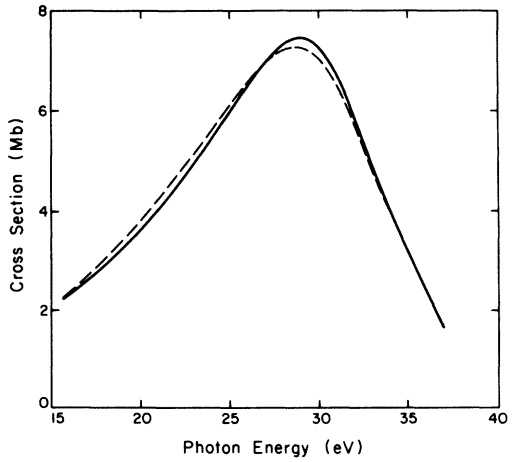

FIG. 2. Convergence of the $3\sigma_g \rightarrow k\sigma_u$ photoionization cross section of N_2 using the iterative Schwinger method: – – – –, iteration zero using Eq. (10); ——, iteration one using Eq. (14).

tion while using only the FCHF approximation for the final state, significantly improved the computed cross section when compared to using only a HF initial-state wave function. In this study we have examined effects of initial-state correlation on the computed photoionization cross sections of molecular nitrogen. As initial-state wave functions we have used the HF wave function described in the previous section and a CI wave function containing "singles-plus-doubles" excitations.[39]

In order to limit the size of the CI wave function, the virtual orbital space was taken to be a restricted set of orbitals. The virtual orbitals were obtained by performing a separated-pair-type MCSCF calculation.[29,40] The orbital occupation in the HF wave function is

$$(1\sigma_g)^2(2\sigma_g)^2(3\sigma_g)^2(1\sigma_u)^2(2\sigma_u)^2(1\pi_{ux})^2(1\pi_{uy})^2 \, . \tag{54}$$

Note that we have performed the initial-state calculations in D_{2h} symmetry. In the separated-pair calculation the valence electron pairs are expanded in orthogonal natural orbitals. The wave function we used for N_2 may be represented as

$$(1\sigma_g)^2(2\sigma_g,5\sigma_g,5\sigma_u)^2(3\sigma_g,4\sigma_g,3\sigma_u,4\sigma_u,3\pi_{ux},3\pi_{uy},3\pi_{gx},3\pi_{gy})^2(1\sigma_u)^2(2\sigma_u,6\sigma_g,6\sigma_u)^2(1\pi_{ux},1\pi_{gx},2\pi_{ux},2\pi_{gx})^2$$
$$(1\pi_{uy},1\pi_{gy},2\pi_{uy},2\pi_{gy})^2 , \tag{55}$$

where the orbital listed within each pair of parentheses represents the natural orbitals of a particular pair function. The energy of this separated-pair wave function for N_2 is $-109.054\,489$ a.u. The orbitals in each pair function which are doubly occupied in the HF approximation were not allowed to vary from their HF form. This constraint made the evaluation of the photoionization cross sections simpler since in matrix elements of the form of Eqs. (41) and (42), this restriction allows only the continuum orbital in the final state to be nonorthogonal to the orbitals in the correlated initial-state wave function. Having only one nonorthogonal orbital in the final state, causes the configurations in the initial-state wave function, differing from the reference HF configuration by three or more spin-orbitals, not to contribute to the photoionization cross section. Hence we have chosen a linear combination of configurations differing from the HF configuration by no more than two orbitals to represent the correlated initial-state wave function. The virtual orbital space was taken to be the set of orbitals determined in the separated-pair calculation. We have also restricted the calculation by requiring the $1\sigma_g$ and $1\sigma_u$ orbitals to remain doubly occupied in all configurations. The resulting wave function has 386 spatial configurations in D_{2h} symmetry, from which 570 spin eigenfunctions are constructed. The energy of this CI wave function is $-109.173\,549$ a.u.

C. Photoionization leading to the $X\,^2\Sigma_g^+$ state of N_2^+

Photoionization leading to the $X\,^2\Sigma_g^+$ state of N_2^+ is of primary interest due to the appearance of a shape resonance in the cross section. In the one-electron picture used here this channel corresponds to photoionization from the $3\sigma_g$ orbital into a continuum orbital of either σ_u or π_u symmetry. The maximum l included in the expansion of the scattering solution [Eq. (7)] is $l_p=7$ for the continuum solutions of σ_u symmetry and $l_p=5$ for continuum solutions of π_u symmetry. The ionization potential we used for this channel was IP = 15.6 eV.[3,11]

There have been several studies of the shape resonance in this channel using the FCHF approximation.[3,9,10] Among these studies there is a disagreement of about 3 eV in the position of the peak photoionization due to the resonance. For the $3\sigma_g \rightarrow k\sigma_u$ channel alone, Rescigno *et al.*[3] obtained a peak cross section at a photon energy of ~ 28 eV, whereas both Raseev *et al.*[9] and Robb and Collins[10] obtained the peak cross section at ~ 31 eV. Figure 2 shows that the peak cross section in our calculation is at ~ 29 eV.

The discrepancy between our peak cross-section energy and those of Raseev *et al.* and Robb and Collins could be due either to the different targets used or the different expansion parameters used. To see if the difference in the targets is important, we have performed a calculation in which we used similar expansion parameters to those used by Raseev *et al.*[9] For this calculation we have taken as our expansion parameters $l_m=13$, $l_s^{\rm ex}=9$, $l_i^{\rm ex}=7$ for all i, $l_i^{\rm dir}=50$, $\lambda_m^{\rm ex}=5$, $\lambda_m^{\rm dir}=14$. Using these parameters we obtain the peak cross-section energy at 30.7 eV. Thus, the difference between using a target wave function constructed from Gaussian functions as in the present study or from Slater-type functions as in the studies by Raseev *et al.*[9] and Robb and Collins[10] is seen to be small. Thus, most of the difference between the results of Raseev *et al.*[9] and Robb and Collins[10] and our present results must be due to the lack of convergence of the expansion parameters in the earlier studies.

In order to examine the behavior of the peak cross section with respect to the l expansion used, we have performed an additional set of calculations. The very small difference between the B and D calculations discussed in Sec. III A indicates that the exchange potential is converged with $l_{\rm max}^{\rm exc}=30$. Thus, the only variations in l that we will consider here are those in $l_{\rm max}^{\rm dir}$. We have thus performed calculations with $l_{\rm max}^{\rm exc}=30$ and $l_{\rm max}^{\rm dir}=34,38,42,46,50$. We have computed the

photoionization cross section for the $3\sigma_g \rightarrow k\sigma_u$ channel at three photoelectron energies, 0.47, 0.50, and 0.53 a.u., which corresponds to photon energies of 28.4, 29.2, and 30.0 eV. Using these three energies we then used polynomial interpolation to obtain the photon energy of the peak cross section. We have plotted the resulting energies against $1/(l_{\max}^{\text{dir}})^3$ in Fig. 3. As can be seen from Fig. 3, the peak energies fall on a straight line when plotted against $1/(l_{\max}^{\text{dir}})^3$. Thus, we have empirically determined the relationship given in Eq. (1), i.e.,

$$E_{\max}^{l} - E_{\max}^{\infty} \propto \frac{1}{l^3} .$$

The extrapolated energy for the peak cross section is then 28.7 eV.

We believe that this functional dependence of the resonance energy on $l_{\max}^{\text{dir}}$ is due to the interaction of resonant function of σ symmetry, which satisfies the appropriate cusp condition at a nucleus, and the nuclear potential at that point. To test this conjecture we computed the potential integral of an s-type Slater function of exponent $\xi = 2.0$, which has the correct cusp condition at its origin, with a point charge at the center of the Slater function. This integral was performed using a single-center expansion about an origin 1.034 a.u. away from the center of the Slater function.[41] Note that this distance is the same as the distance from the expansion center to the nuclei in nitrogen. The convergence of this integral with $l_{\max}$ was also found to obey the law given in Eq. (1), suggesting that this $1/l^3$ convergence could be general for all σ shape resonances, although we do not have a rigorous proof of this. We have also observed this rate of convergence in the $4\sigma_g \rightarrow k\sigma_u$ photoionization resonance in CO_2.[19(b)] Note that for resonances with $m \neq 0$ (π, δ, etc.) the convergence behavior will be different, and one would expect these resonance energies to converge faster with increasing l than did the σ resonance discussed here.

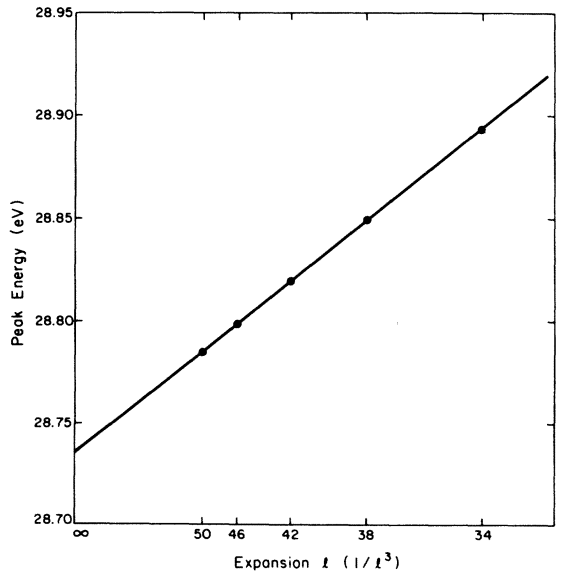

FIG. 3. Dependence of the energy of the peak photoionization cross section on $l_{\max}^{\text{dir}}$ for the $3\sigma_g \rightarrow k\sigma_u$ channel of N_2.

In Fig. 4 we give the total cross section leading to the $X\,^2\Sigma_g^+$ state of N_2^+. We have plotted the computed dipole length and dipole velocity cross sections, using both the HF and CI intitial-state wave functions, along with the experimental results of Plummer *et al.*[11] and of Hamnett *et al.*[13] As in studies of atomic photoionization by Swanson and Armstrong,[22] the correlated intitial-state wave function brings the length and velocity forms of the cross section closer together in better agreement with the experimental results.

The feature at 23 eV in the experimental cross section has been attributed to autoionization from Rydberg states leading to the $C\,^2\Sigma_u^+$ state of

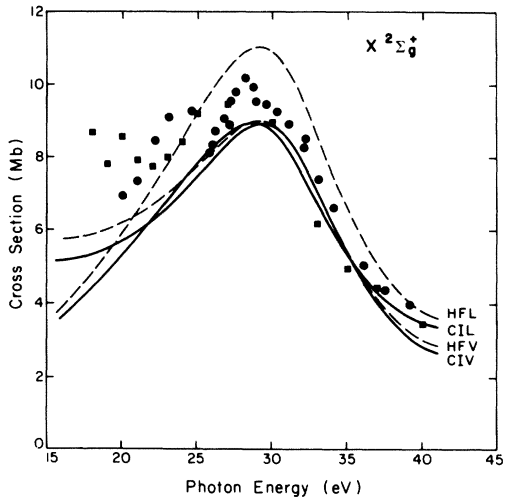

FIG. 4. Photoionization cross section for the production of the $X\,^2\Sigma_g^+$ state of N_2^+: HFL, in the dipole length approximation using a Hartree-Fock initial-state wave function; HFV, in the dipole velocity approximation using a Hartree-Fock initial-state wave function; CIL, in the dipole length approximation using a configuration-interaction intitial-state wave function; CIV, in the dipole velocity approximation using a configuration initial-state wave function; ●, experimental results of Plummer *et al.* (Ref. 11); ■, experimental results of Hamnett *et al.* (Ref. 13).

N_2^+.[11,42] To obtain such autoionization features, theoretically, one would have to include final-state effects not present in the FCHF model used here.

In Fig. 5 we present our computed ITAD and IDAD asymmetry parameters. The effect of initial-state correlation on the computed β's is small. Thus, for all the asymmetry parameters reported here, we will only present our most reliable results obtained using the CI initial-state wave function. The computed ITAD asymmetry parameters agree well with the experimental results of Marr *et al.*,[12] except for the values around the feature at 23 eV and at lower energies where autoionization features are important. We note that there are no dramatic changes in the $\beta_{\hat{k}}$ values in the resonance region in contrast to the significant $\beta_{\hat{k}}$ effects which have been predicted in the $4\sigma_g \rightarrow k\sigma_u$ photoionization resonance in CO_2.[19(b),43] The results for the IDAD asymmetry parameter show that above the resonance energy the contribution from the $k\sigma_u$ continuum channel drops off rapidly leaving only the contribution from the $k\pi_u$ continuum.

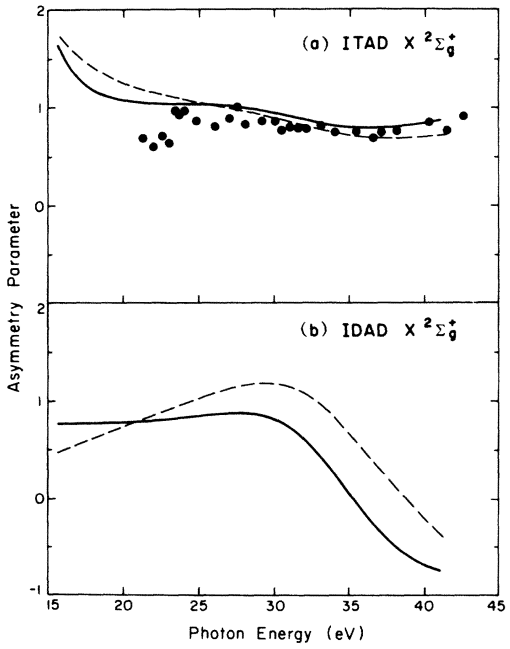

FIG. 5. Photoionization asymmetry parameters for the production of the $X\,^2\Sigma_g^+$ state of N_2^+:
(a) ITAD asymmetry parameter $\beta_{\hat{k}}$; (b) IDAD asymmetry parameter $\beta_{\hat{n}}$; ——, dipole length approximation using a correlated initial state; — — — —, dipole velocity approximation using a correlated initial-state wave function; ●, experimental $\beta_{\hat{k}}$ of Marr *et al.* (Ref. 12).

D. Photoionization leading to the $A\,^2\Pi_u$ state of N_2^+

The photoionization channel leading to the $A\,^2\Pi_u$ state of N_2^+ corresponds in the one-electron picture to ejecting an electron from the $1\pi_u$ orbital into a continuum orbital having σ_g, π_g, or δ_g symmetry. For the ionization potential of this channel we have used IP = 16.7 eV.[3,11] The maximum l included in the expansion of the scattering solution [Eq. (7)] was $l_p = 6$ for continuum solutions of σ_g, π_g, and δ_g symmetries.

There is a well-known difficulty associated with using the FCHF approximation for the $1\pi_u \rightarrow k\pi_g$ channel.[4,5] If the straightforward FCHF potential is used, the photoionization cross section is unphysically large as shown in Fig. 6(a). The potential used in this calculation was the usual singlet-coupled potential for the $\pi_u^3 k\pi_g$ configuration

$$V_\pi^1 = \sum_\sigma (2J_\sigma - K_\sigma) + 2J_{\pi^-} + J_{\pi^+} + K_{\pi^+} - K_{\pi^-} + 2S'_\pi - S''_\pi \,, \tag{56}$$

where J and K are the usual Coulomb and exchange operators, and S' and S'' are defined by

$$S'_\pi \phi^+(\vec{r}_1) = \pi^+(\vec{r}_1) \int d^3r_2 \frac{[\pi^-(\vec{r}_2)]^* \phi^-(\vec{r}_2)}{r_{12}} \tag{57}$$

and

$$S''_\pi \phi^+(\vec{r}_1) = \phi^-(\vec{r}_1) \int d^3r_2 \frac{[\pi^-(\vec{r}_2)]^* \pi^+(\vec{r}_2)}{r_{12}} \,. \tag{58}$$

The origin of the unphysical result presented in Fig. 6(a) is that the HF potential given in Eq. (56) places the strong valence $\pi \rightarrow \pi^*$ transition above the ionization threshold. This transition then appears as a large feature in the photoionization profile. If the appropriate $\sigma \rightarrow \sigma^*$ correlations were included in the final-state wave function, then this transition would be brought below the ionization threshold in better agreement with experiment.[5] Instead of including final-state correlation in our calculation, we have chosen to modify the HF potential so that the $\pi \rightarrow \pi^*$ oscillator strength is removed from the continuum.[4] We have tried three different ways of removing this deficiency of the HF potential.

The first two methods are based on the observation that if an appropriate representation could be found for the π^* orbital, then the continuum solutions could be obtained using the singlet potential given in Eq. (56), with the additional condition

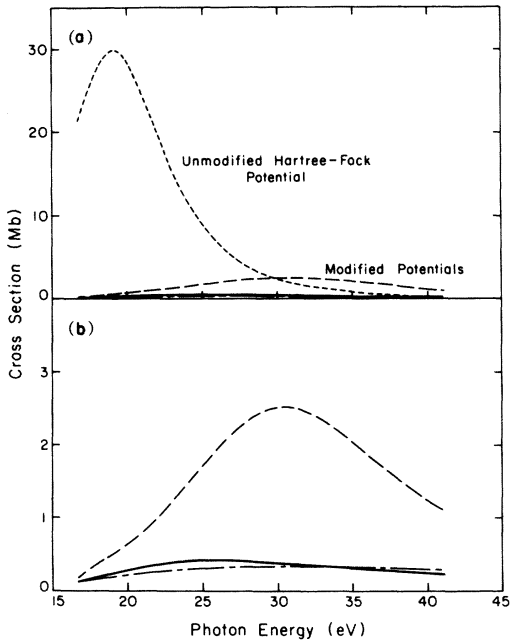

FIG. 6. Photoionization cross sections in the $1\pi_u \rightarrow k\pi_g$ channel of N_2 using various forms for the scattering potential: (a) unmodified potential compared with modified forms; (b) expanded scale showing modified potentials; ——, the cross section obtained using continuum solutions which are eigenfunctions of the triplet Hartree-Fock potential; — - — -, using eigenfunctions of the singlet Hartree-Fock potential constrained to be orthogonal to a valence π_g eigenfunction of the triplet Hartree-Fock potential; — — — —, using eigenfunctions of the singlet Hartree-Fock potential constrained to be orthogonal to a valence π_g eigenfunction of the singlet Hartree-Fock potential; ----- , using eigenfunctions of the unmodified singlet Hartree-Fock potential.

that the continuum solution be orthogonal to the valence π^* orbital.[4] The orthogonality condition is imposed by using the appropriate Phillips-Kleinman potential. We have obtained the valence π^* orbital using two methods. The first method used was to obtain eigenfunctions of the singlet potential using only a valence basis set. For this calculation we used the same basis set as was used to obtain the HF wave function. The eigenavalue of the π_g^* orbital using the singlet potential was 2.08 eV. The second is to construct eigenfunctions of the triplet potential

$$V_\pi^3 = \sum_\sigma (2J_\sigma - K_\sigma) + 2J_{\pi^-} + J_{\pi^+} - K_{\pi^+} - K_{\pi^-} - S_\pi'' \ . \quad (59)$$

The eigenvalue of the π_g^+ orbital in our valence basis set for this potential was -10.15 eV. This eigenvalue corresponds to an excitation energy of 6.49 eV for the transition to the $A\ ^3\Sigma_u^+$ state N_2.[44] Using the triplet π^* orbital and projected singlet potential was the original solution to this problem used by Rescigno *et al.*[4] An alternative to using the projected singlet potential is to use the triplet potential given in Eq. (59) directly to obtain the continuum solutions. The use of the triplet potential to solve the $\pi \rightarrow \pi^*$ problem has been used by Padial *et al.* in photoionization studies of CO_2.[45] The photoionization cross sections obtained using these three modifications to the FCHF approximation are presented in Fig. 6(b). We see that the triplet orbital with projected singlet scattering potential gives results very similar to those obtained from the triplet scattering potential. The singlet orbital with projected singlet scattering potential does not seem to be as satisfactory as the other two methods. This probably implies that the valence singlet π^* orbital has been contaminated by nonvalence contributions. The rest of the results for this channel were obtained using the triplet scattering potential, which seems to be the simplest approach to avoiding the $\pi \rightarrow \pi^*$ problem.

In Fig. 7 we present the cross sections for photoionization leading to the $A\ ^2\Pi_u$ state. We give results obtained using the dipole length and dipole velocity forms of the cross section using both HF- and CI-type initial-state wave functions. We compare our results to the experimental data of Plummer *et al.*[11] and of Hamnett *et al.*[13] In this channel the effect of using a CI initial-state wave function is not very large. Inclusion of initial-state correlation does bring the length and velocity cross sections into slightly better agreement, however, the effect is not as large as we found in the channel leading to the $X\ ^2\Sigma_g^+$ state of N_2^+. In the experimental cross section the feature at 23 eV is again due to autoionization from Rydberg states leading to the $C\ ^2\Sigma_u^+$ state of N_2^+.[11,42]

The broad peaked shape of the cross section in this channel is due to the $1\pi_u \rightarrow k\delta_g$ channel. The enhancement of the cross section in this channel is examined in more detail in Fig. 8 where the cross section and eigenphase sums of the $1\pi_u \rightarrow k\delta_g$ channel are compared to those of the resonant $3\sigma_g \rightarrow k\sigma_u$ channel. As can be seen from Fig. 8, the peak of the $1\pi_u \rightarrow k\delta_g$ cross section is very broad when compared to the $3\sigma_g \rightarrow k\sigma_u$ cross section. Also, the eigenphase sums indicate that the $1\pi_u \rightarrow k\delta_g$ channel is not resonant. Thus, the nonresonant energy dependence of the dipole matrix

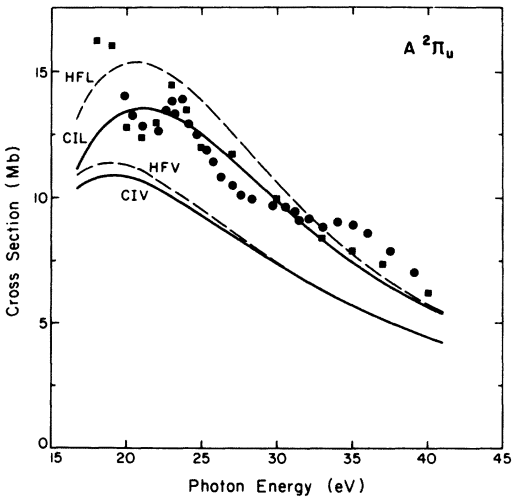

FIG. 7. Photoionization cross section for the production of the $A\ ^2\Pi_u$ state of N_2^+ (same designations as in Fig. 4).

elements must determine the shape of the $1\pi_u \rightarrow k\delta_g$ photoionization cross section of N_2 in much the same manner as it does the shape of the $2p \rightarrow kd$ photoionization cross section of Ne, as discussed by Cooper.[46]

We present in Fig. 9 the asymmetry parameters for this channel. Once again our computed β_k

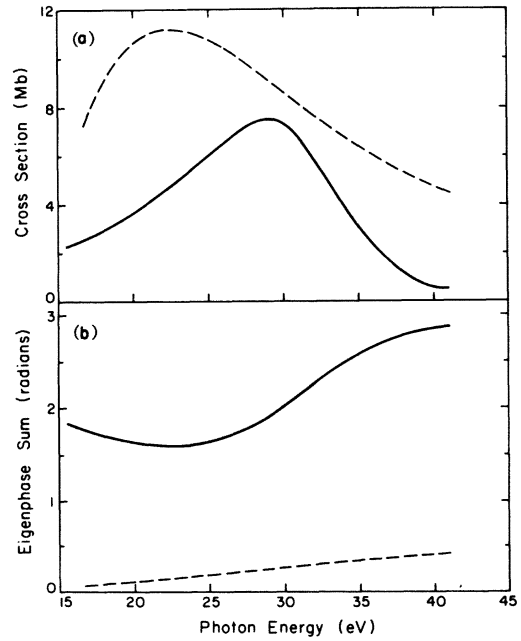

FIG. 8. Comparison of photoionization in the $3\sigma_g \rightarrow k\sigma_u$ channel with photoionization in the $1\pi_u \rightarrow k\delta_g$ channel of N_2: (a) comparison of photoionization cross sections; (b) comparison of eigenphase sums; ——, $3\sigma_g \rightarrow k\sigma_u$ channel; — — — —, $1\pi_u \rightarrow k\delta_g$ channel.

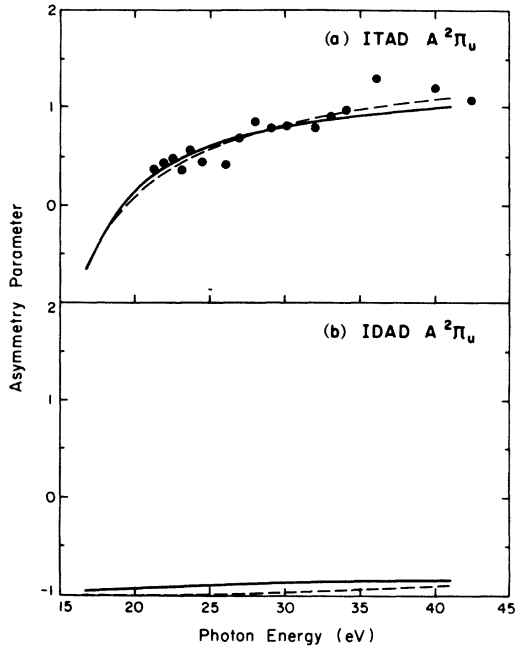

FIG. 9. Photoionization asymmetry parameters for the production of the $A\ ^2\Pi_u$ state of N_2^+ (same designations as in Fig. 5).

agrees well with the experimental results of Marr *et al.*[12] The computed $\beta_{\hat{n}}$, which is very near in value to -1, reflects that the $\mu=0$ contribution ($1\pi_u \rightarrow k\pi_g$) is very small.

E. Photoionization leading to the $B\ ^2\Sigma_u^+$ state of N_2^+

In the one-electron picture, the photoionization channel leading to the $B\ ^2\Sigma_u^+$ state of N_2^+ corresponds to ejecting an electron from the $2\sigma_u$ orbital into a continuum orbital of σ_g or π_g symmetry. We used 18.8 eV for the ionization potential of this state.[3,11] The maximum l included in the expansion of the scattering solution [Eq. (7)] was $l_p=6$ for continuum solutions of both σ_g and π_g symmetry.

In Fig. 10 we present the calculated cross sections for this channel. In this case there seems to be little differential effect between length and velocity forms of the cross section on going from the HF initial-state wave function to the CI wave function. We also see in Fig. 10 that the present results are in fairly good agreement with the experimental results of Plummer *et al.*[11] and with those of Hamnett *et al.*[13]

In Fig. 11 we present the β's for this channel. The agreement between the calculated β_k and the experimental points of Marr *et al.*[12] is not satisfac-

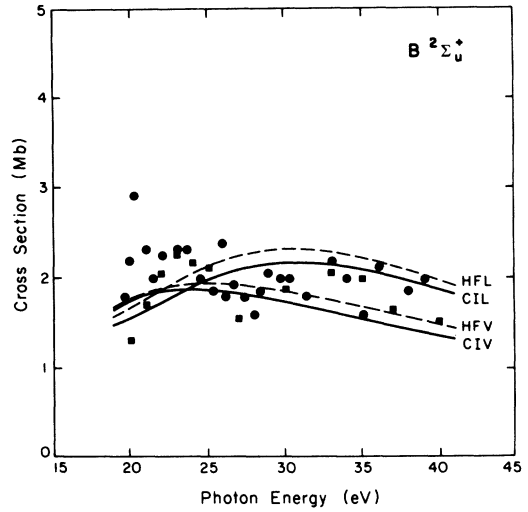

FIG. 10. Photoionization cross section for production of the $B\,^2\Sigma_u^+$ state of N_2^+ (same designations as in Fig. 4).

tory in this channel as it was in the other two channels we have considered here. This difficulty is probably due to the inadequacy of the single-particle hole state used in the FCHF approximation for this higher-energy ionic state. A more accurate treatment would necessarily include a better representation of the final-state ionic wave function. The computed β_{fi} reflects that at low energy

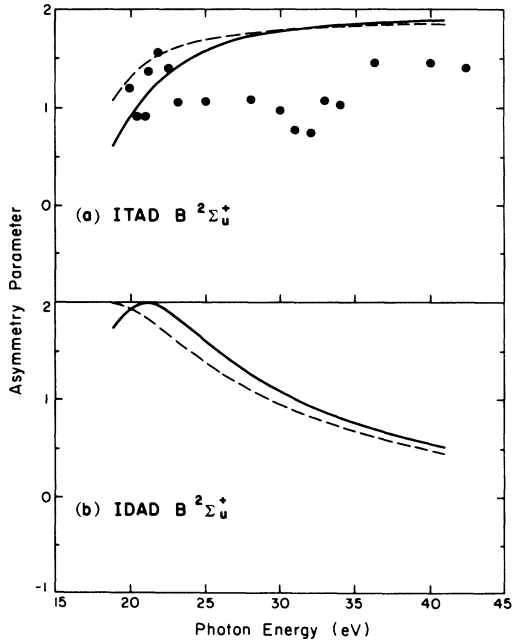

FIG. 11. Photoionization asymmetry parameters for the production of the $B\,^2\Sigma_u^+$ state of N_2^+ (same designations as in Fig. 5).

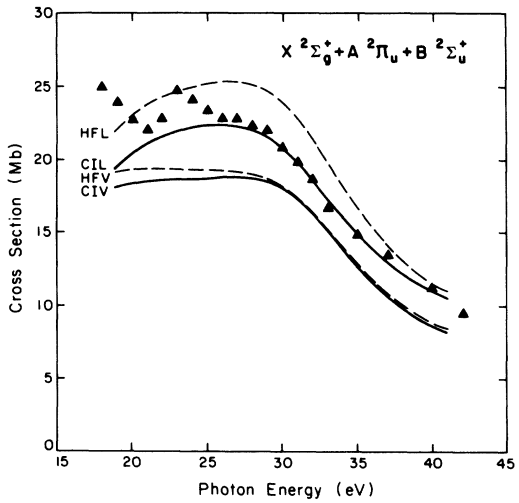

FIG. 12. Total photoionization cross section for the production of the $X\,^2\Sigma_g^+$, $A\,^2\Pi_u$, and $B\,^2\Sigma_u^+$ states of N_2^+ (same designations as in Fig. 4): ▲, total experimental cross sections of Wight *et al.* (Ref. 14) corrected to only include the contribution from these three channels using the experimental branching ratios of Hamnett *et al.* (Ref. 13).

the main contribution to the cross section is from the $2\sigma_u \rightarrow k\sigma_g$ channel, and that at higher energy the $2\sigma_u \rightarrow k\pi_g$ channel becomes more important.

F. Total photoionization cross section of N_2

We have summed the cross sections discussed above to obtain the total photoionization cross section of N_2 leading to the $X\,^2\Sigma_g^+$, $A\,^2\Pi_u^+$, and $B\,^2\Sigma_u^+$ states of N_2^+. These results are presented in Fig. 12 along with the total ionization cross sections obtained by Wight *et al.*[14] In order to make an appropriate comparison with our total cross section, we have corrected Wight's total cross section by multiplying by the sum of the branching ratios, obtained by Hamnett *et al.*,[13] for the three channels we have considered.

We can see from Fig. 12 that the effect of initial-state correlation is to lower the length form and not to alter appreciably the velocity form of the cross section. The length form is now in excellent agreement with experimental results except for the 23-eV feature which we mentioned earlier. In particular, the shape of the shoulder in the cross section due to the $3\sigma_g \rightarrow k\sigma_u$ resonance, as well as the high-energy falloff of the cross section, are well reproduced using the FCHF model with initial-state correlation included.

It seems that the total calculated cross section is

in better agreement with the experimental results than are the individual partial channel cross sections. This is probably due to effects of interchannel coupling which might redistribute the oscillator strength between different channels but does not seem to greatly affect the total cross section.

G. Comparison with other theoretical methods

The partial cross sections for the three channels, which we have considered here, have been studied previously using the CMSM (Ref. 2) and STMT (Refs. 3 and 4) approaches to photoionization. In Fig. 13 we have compared our FCHF results obtained in the dipole length approximation using a HF initial-state wave function with results from the CMSM and STMT methods. The three methods are in qualitative agreement. The STMT results seem to be within 10—15% of our single-center results. The CMSM results are generally in worse agreement with the single-center results than are the STMT results.

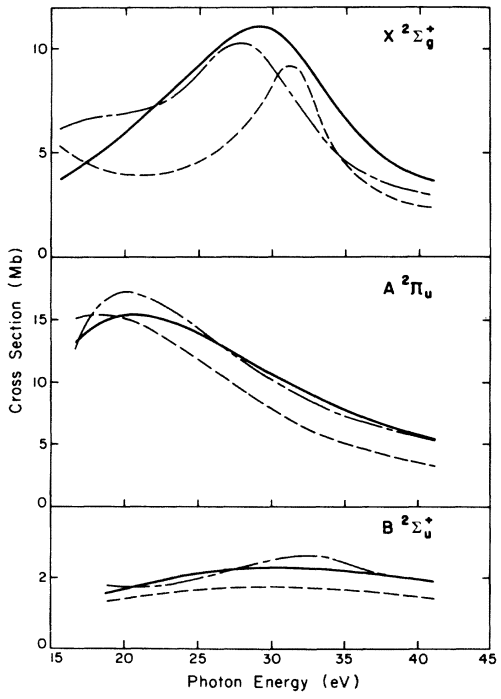

FIG. 13. Comparison of different theoretical cross sections for the production of the $X\,^2\Sigma_g^+$, $A\,^2\Pi_u$, and $B\,^2\Sigma_u^+$ states of N_2^+: ——, present single-center FCHF results; — · —, FCHF results obtained using the STMT approach (Refs. 3 and 4); — — —, CMSM model potential results (Ref. 2).

V. CONCLUSIONS

We have obtained photoionizatin cross sections of N_2 using a single-center expansion technique, and examined in detail the effect of the truncation of the single-center expansion on the energy of the peak cross section in the $3\sigma_g \rightarrow k\sigma_u$ channel. We found that the peak energy for this resonance converged as $1/l^3$. This rate of convergence was also found in single-center expanded nuclear potential integrals, where the orbitals involved were of σ symmetry. Thus the $1/l^3$ convergence may be a general feature of σ symmetry shape resonances.

The coupled integral equations resulting from the single-center expansion of the Lippmann-Schwinger equation were solved using the iterative Schwinger variational method. We found that, with an adequate initial basis set, the iterative method converged to accurate static-exchange results in only one iteration.

We have used a frozen-core Hartree-Fock final state with a correlated initial state to compute molecular photoionization cross sections. This combination gives a good representation of the photoionization process except when two-electron resonances are important. We feel that it is important to obtain these accurate HF level final-state solutions before attempting to treat final-state correlation effects.

ACKNOWLEDGMENTS

This material is based upon work supported by the National Science Foundation under Grant No. CHE 79-15807. This research was also supported in part by an Institutional Grant from the United States Department of Energy Grant No. EY-76-G-03-1305. The research reported in this paper made use of the Dreyfus-NSF Theoretical Chemistry Computer which was funded through grants from the Camille and Henry Dreyfus Foundation, the National Science Foundation (Grant No. CHE 78-20235), and the Sloan Fund of the California Institute of Technology. We thank Professor W. A. Goddard III for making his molecular bound-state computer codes available and J. Low for help with these programs. One of us (R.R.L.) acknowledges support from a National Science Foundation Graduate Research Fellowship and from an Exxon Foundation Graduate Educational Fellowship. One of us (G.R.) acknowledges a fellowship from IBM (Belgium).

*Present address: Département de Chimie Générale et Physique, Bâtiment B6, Université de Liège, Sart-Tilman, B-4000 Liège 1, Belgium.

[1]See, for example, *Electron-Molecule and Photon-Molecule Collisions,* edited by T. Rescigno, V. McKoy, and B. Schneider (Plenum, New York, 1979).

[2]J. W. Davenport, Phys. Rev. Lett. 36, 945 (1976); Int. J. Quantum Chem. S11, 89 (1977).

[3]T. N. Rescigno, C. F. Bender, B. V. McKoy, and P. W. Langhoff, J. Chem. Phys. 68, 970 (1978).

[4]T. N. Rescigno, A. Gerwer, B. V. McKoy, and P. W. Langhoff, Chem. Phys. Lett. 66, 116 (1979).

[5]G. R. J. Williams and P. W. Langhoff, Chem. Phys. Lett. 78, 21 (1981).

[6]A. Temkin and K. V. Vasavada, Phys. Rev. 160, 109 (1967).

[7]F. Hirota, Chem. Phys. Lett. 74, 67 (1980).

[8]C. Duzy and R. S. Berry, J. Chem. Phys. 64, 2421 (1976).

[9]G. Raseev, H. LeRouzo, and H. Lefebvre-Brion, J. Chem. Phys. 72, 5701 (1980).

[10]W. D. Robb and L. A. Collins, Phys. Rev. A 22, 2474 (1980).

[11]E. W. Plummer, T. Gustafsson, W. Gudat, and D. E. Eastman, Phys. Rev. A 15, 2339 (1977).

[12]G. V. Marr, J. M. Morton, R. M. Holmes, and D. G. McCoy, J. Phys. B 12, 43 (1979).

[13]A. Hamnett, W. Stoll, and C. E. Brion, J. Electron Spectrosc. Relat. Phenom. 8, 367 (1976).

[14]G. R. Wight, M. J. Van der Wiel, and C. E. Brion, J. Phys. B 9, 675 (1976).

[15]S. Wallace and D. Dill, Phys. Rev. B 17, 1692 (1978).

[16]R. R. Lucchese, D. K. Watson, and V. McKoy, Phys. Rev. A 22, 421 (1980).

[17]R. R. Lucchese, K. Takatsuka, D. K. Watson, and V. McKoy, *The Schwinger Variational Principle: An Approach to Electron-Molecule Collisions, in Proceedings of the Symposium on Electron-Atom and Molecule Collisions, Universitat Bielefeld* (Plenum, London, 1981).

[18]R. R. Lucchese and V. McKoy, Phys. Rev. A 24, 770 (1981).

[19](a) R. R. Lucchese and V. McKoy, J. Phys. Chem. 85, 2166 (1981); (b) R. R. Lucchese and V. McKoy (unpublished).

[20]D. K. Watson, T. N. Rescigno, and B. V. McKoy, J. Phys. B 14, 1875 (1981).

[21]R. R. Lucchese and V. McKoy, Phys. Rev. A (in press).

[22]J. R. Swanson and L. Armstrong, Jr., Phys. Rev. A 15, 661 (1977).

[23]M. Abramowitz, in *Handbook of Mathematical Functions,* Appl. Math. Series 55, edited by M. Abramowitz and I. A. Stegun (National Bureau of Standards, Washington, D. C., 1972), p. 537.

[24]G. Arfken, *Mathematical Methods for Physicists,* 2nd ed. (Academic, New York, 1970), p. 737.

[25]W. H. Miller, J. Chem. Phys. 50, 407 (1969).

[26]S. K. Adhikari and I. H. Sloan, Phys. Rev. C 11, 1133 (1975).

[27]V. B. Belyaev, A. P. Podkopoyev, J. Wrzecionko, and A. L. Zubarev, J. Phys. B 12, 1225 (1979).

[28]M. E. Riley and D. G. Truhlar, J. Chem. Phys. 65, 792 (1976).

[29]F. W. Bobrowicz and W. A. Goddard III, in *Modern Theoretical Chemistry 3,* edited by H. F. Schaefer III (Plenum, New York, 1977), p. 79.

[30]R. R. Lucchese and V. McKoy, Phys. Rev. A 21, 112 (1980).

[31]P. G. Burke and N. Chandra, J. Phys. B 5, 1696 (1972).

[32]J. D. Weeks, A. Hazi, and S. A. Rice, in *Advances in Chemical Physics, Vol. XVI* (Interscience, New York, 1969), p. 283.

[33]H. P. Kelly, Chem. Phys. Lett. 20, 547 (1973).

[34]J. C. Tully, R. S. Berry, and B. J. Dalton, Phys. Rev. 176, 95 (1968).

[35]T. H. Dunning, Jr., J. Chem. Phys. 53, 2823 (1970).

[36]T. H. Dunning, Jr., J. Chem. Phys. 55, 3958 (1971).

[37]A. W. Fliflet and V. McKoy, Phys. Rev. A 18, 1048 (1978).

[38]L. A. Collins, W. D. Robb, and M. A. Morrison, Phys. Rev. A 21, 488 (1980).

[39]I. Shavitt, in *Modern Theoretical Chemistry 3,* edited by H. F. Schaefer III (Plenum, New York, 1977), p. 189.

[40]D. M. Silver, E. L. Mehler, and K. Ruedenberg, J. Chem. Phys. 52, 1174 (1970).

[41]F. E. Harris and H. H. Michels, J. Chem. Phys. 43, S165 (1965).

[42]K. Codling, Astrophys. J. 143, 552 (1966).

[43]F. A. Grimm, T. A. Carlson, W. B. Dress, D. Agron, J. O. Thomson, and J. W. Davenport, J. Chem. Phys. 72, 3041 (1980).

[44]J. B. Rose and V. McKoy, J. Chem. Phys. 55, 5435 (1971).

[45]N. Padial, G. Csanak, B. V. McKoy, and P. W. Langhoff, Phys. Rev. A 23, 218 (1981).

[46]J. W. Cooper, Phys. Rev. 128, 681 (1962).